JOURNAL OF NORTHEASTERN UNIVERSITY

Volume 25 Issue 04, 2022 ISSN: 1005-3026 https://dbdxxb.cn/ Original Research Paper

CHARACTERISTICS OF WILLIAMSON-CASSON-NANOFLUID FLOW ACROSS AN IMPERMEABLE EXTENDING THE SHEET IN THE EXISTINGOF HEAT TRANSFER MELTING AND ELECTROMAGNETIC FIELD

R. Vijaya Kumar* , R. S. Durga Rao[1]and V. Vasudeva Murthy[2]

* Mathematics Section, FEAT,Annamalai University, Annamalainagar - 608 002, India.

Department of Mathematics, Periyar Arts College, Cuddalore, 607001, Tamilnadu State, India.

1 Department of Mathematics, Vishnu Institute of Technology, Bhimavaram,West Godavari (Dt), 534201,

Andhra Pradesh, India.

2 Department of Mathematics, S. R. K. R. Engineering College, Bhimavaram, West Godavari (Dt), 534201,

Andhra Pradesh, India.

*Corresponding author Email address: rathirath_viji@yahoo.co.in

Abstract: For this work, scientists examined the behaviour that is not Newtonian Williamson-Casson-Williamson nanofluid in contact with a porous substance and a magnetic field as it flows towards an impermeable, stretched sheet. We investigate the thermophoresis and Brownian motion phenomena that arise when a non-linearly stretched sheet undergoes melting heat transfer.Consideration is given to the stages below to make the implementation of computational algorithms practical.

a) Using the appropriate transformation, the PDEs are turned into ODEs.
b) This results in a boundary value issue, which then leads to an initial value issue.
c) Using the Runge-Kutta technique, these built ordinary differential equations are computationally solved.
d) Using both graphical output and tabular data, the impact logs of a physical flow parameter are analysed.
e) In addition, tables are used to calculate the different Sherwood, Nusselt, and skin-friction numbers.
f) The accuracy of the current procedure and that of previously published research are highly concordant.

Keywords: Williamson fluid; Casson fluid; Nanofluid; Porous medium; Melting transfer; Magnetic field; Impermeable stretching sheet;

Nomenclature

List of Symbols

: Components of Velocity in the directions ofx and y respectively (m/s)
: Calculated Cartesian coordinates in along the stretching sheet,(m)
: Function of a dimensionless stream

Submitted: 21/10/2022 **Accepted**: 24/11/2022

: velocity of the Fluid(m/s)
: Prandtl number
: Volume concentration of fluid nanoparticles (mol / m3)
: Fluid temperature (K)
: Origin
: Dimensional ambient volume fraction (mol / m3)
: Dimensional concentration of nanoparticles at the stretched surface (mol / m3)
: Nanofluid temperature close to the wall (K)
: A persistent magnetic field (Tesla)
: Magnetic field parameter
: Temperature Fluid distant from the stretched sheet (K)
: Coefficient of Skin-friction (s-1)
: Parameter for Brownian motion
: The fluid Stretching velocity (m/s)
: Coefficient of heat transfer rate (or) Nusselt number
: Parameter Thermophoresis
: Parameter Lewis number
: Coefficient of Heat flux
: Coefficient of Mass flux
: Nano particles Specific heat capacity (J / kg / K)
: Coefficient of Brownian diffusion
: Thermophoresis Diffusion Coefficient(m2/ s)
: Mass transfer Coefficientrate (or)Sherwood number
: Parameter of the Permeability (m-1)
: The porous medium's permeability (m-1)
: Positive real number
: Reynold's number
: Melting heat transfer parameter
: Melting surface temperature (K)
: Concentration susceptibility
: Reference temperature (K)

Greek symbols

: Molecular mean free path
: Similarity Dimensionless variable (m)
: temperature in Non-dimensional (K)
: Nanoparticle concentrationin Non-Dimensional (mol / m3)

: Heat transferivity, (m2 / s)
: Motion viscosity, (m2 / s)
: Stefan-Boltzmann constant,
(W . m-2. K-4)
: Density of the fluid, (kg / m3)
: The fluid‘s Dynamic viscosity ,
: Thermal conductivityfluid,
(W / (m·K))
: Parameter of Casson fluid
: Williamson Parameter fluid
: Stream function
: TensorofCauchyStress
: Dynamic viscosity of Casson fluid
(m2/s)
: Shear rate
: Shear stress
Superscript
: Derivative with regard to
Subscripts
: Fluid,
: state of the sheet,
: Environmental Factors.

1. Introduction:

The vast potential uses of nanoparticles in fields like biology, optics, and electronics have piqued the curiosity of the scientific community. Particles in nanotechnology are minuscule objects that have their own unique properties and behaviours. Particles are continually separated into coarse and fine categories based on particle size. A coarse particle's size might be anything from 10,000 to 2,500 nm. Small particles range in size from around 2,500 to 100 nano-meters. Nanofluid, which describes a heat transfer fluid in which nanoparticles are dispersed, was first used by Choi [1] including water, ethylene glycol, and other liquids. The basic concept is to add nanoparticles to base fluids in order to increase their heat-transfer efficiency. Engine cooling, heat exchanger efficiency, solar collector cooling, microelectronics, machining, pharmaceutical processing, and vehicle thermal management are just some of the areas where nanofluids may be used to improve heat transfer capacity. Using a stretchy nonlinear surface and a border condition for convection, Hayat et al. [2] examined how a magnetic field affected a pair-stress nanofluid's three-dimensional flow. Nanofluid motion across an extendedsheet was looked into by Zargartalebi et al. [3] at the natural convection stagnation point under the influence of several thermophysical factors.Nadeem et al. [4] examineda magnetic field's effectscovering a nanofluid with an arc viscous flowin two dimensions. With a vertical plate and convective boundary conditions, Ram Reddy et al.[5]

analysed combined heat, mass transfer and convection flowusing nanofluid.Size, shape, base fluid, nanofluid, and base fluid operating temperature were all assessed by Zaraki et al. [6] in their study of convection heat, mass, and boundary layer movement of nanofluids.Using a heated square box of a double-sided top, Tiwari et al. [7] shown how nano-fluids may speed up heat transmission. The cone-shaped vertical flow of natural convection boundary in nanofluid layers via porous surfaces was researched by Gorla et al. [8]. Nadeem et al. [9] found thatnanofluidflowwith it a convective non-aligned stagnation point flow is caused by stretching a sheet with a partial slip effect..A mathematical simulation of a nanofluid flowing through a square hole a porous substance was demonstrated by Sheremet et al. [10].Haq et al. [11] looked at the temperature-related qualities that carbon nanotubes in a magnetically driven sheet flow. While studying the flow, heat and mass transfer in a natural with MHD an outer layer convection, Sudarsana Reddy et al. [12] by usinga vertical cone enmeshed in saturated porous media with nanofluid to account for chemical reaction and thermal radiation. Under boundary conditions for convection, Makinde et al. [13] used an analytical model to examine the nanofluidflow in a sheet that has been stretched.Non-Darcy free convective nanofluid was created by Chamkha et al. [14] using suction/injection, internal heat production, and convection to move down a vertical plate. Natural convection may be used to move the Cu-water nanofluid in the work of Abu-nada et al. [15] in inclined, two-dimensional enclosures.

Research on the movement of non-Newtonian fluids caused by stretched surfaces is and will remain important. This is due to its importance in almost every aspect of engineering and manufacturing today. Common examples of non-Newtonian fluids include shampoos, tomato ketchup, pulps, and sugar solutions. Due to non-linear connection between shear stresses and the rate of deformation, it is hard to fully characterise fundamental characteristics of non-Newtonian fluid models. As a result, predicting the behaviour of non-Newtonian fluids is challenging. Scientists have suggested many various ways for describing the movement of fluids that aren't Newtonian, including fluid model of the Maxwell (1867), the fluid model by Barus (1893), the Bingham Herschel-Bulkly (1922), The power law model by Ostwald-de Waele(1923), the Eyring dynamic model (1936), the Burgers fluid model (1939), the Generalized Burgers (1939), the Reiner-Rivlin fluid model (1945), and the Oldroyd-A (1919) Only the Williamson model can be accurately defined as a fluid with pseudoplastic characteristics among these fluid models of non-Newtonian. For the model of Williamson model, this is an important difference. The Williamson model of fluid dynamics may also identify shear-thinning phenomena. Polymers, melts/solutions, whipped cream, paint, and ketchup are only a few examples of liquids used in industry and biology that stick to the Williamson fluid. Blood is another substance that is drawn to fluid of Williamson. Pseudo-plastic physiologies with minimum and maximum viscosity effects may be described using a model proposed by Williamson [16]. Results from experiments by Bhatti et al. [17] show that Gyrotactic Microorganism affected the motion of MHD Williamson nanofluid as it passed by the rotating discs. Joule heating and Williamson nanofluid flow with negligible mass flux of nanoparticles was investigated by Loganathan and Rajan in [18]. Sreedevi and Reddy [19] studied the flow of Williamson hybrid nanofluid across the spinning cylinder using the

gyrotactic microbe and the Cattaneo-Christov heat flux. Amer [20] used Williamson nanofluids in numerical simulations of heat transfer flow including MHD and thermal radiation. Both of these simulations passed with flying colours. Using the flow of nanofluids generated by a convective boundary and a stretched surface, Yahya et al. [21] nvestigation of Williamson Sutter's response to Cattaneo-Christov heat fluxand.bio-convection. This was done to provide some insight on the link between Williamson Sutter and the two sources of heat. Heat We explore the transfer of a fluid of the Williamson type on a curved porous surface that is exponentially stretched in a magnetohydrodynamic (MHD) mixed convection flow by Ahmed et al. [22]. Through the use of a cylindrically rotating, Aldabesh et al. [23] examine the gyrotactic bacteria effect on a Williamson nanofluid with erratic flow. Krishnamurthy et al. [24] examined the chemical reactivity and thermal radiation and MHD Williamson nanofluid when delivered through porous media. Kumaran et al. [25] studied dissipation of viscosityeffect andheat transmission on through the top paraboloid of rotation, radiative MHD Williamson fluid flow.We investigated the three-dimensional flow Darcy-Forchheimer Williamson nanofluid across a stretched surface in a convective environment in the greatest detail by Dawar et al. [26]. Entropy amplification and activation energy are two novel concepts suggested by Azam et al. [27] for the transient axi-symmetric flow of Williamson nanofluid. Raju et al. [28] used a stretched sheet to approximatively model Williamson and Casson fluid flow, accounting for mass and heat transfer while the fluid flow was modulated by a temperature-dependent heat source. After some debate, Shafiq and Sindhu [29] suggested a non-compressible, unstable Williamson flow. Nazir et al. [30] employed generalised using non-Fourier models investigate mass and heat transmission in a fluid of Williamson.

Casson-Williamson fluid flow problem past a linearlynot impermeable stretched sheet under the melting heat transfer effect, field of magnetic, Thermophoresis, Brownian motion, and porous material has not been studied, the authors note. Therefore, this phenomenon is dealt with in the present paper. The specific aims of this numerical study are as follows.

a) To develop a mathematical model for the results of heat transfer during melting and porous media with the MHD flow Nano-Casson-Williamson fluid behaviour over a stretched, impermeable sheet.

b) A numerical simulation of the flow-controlling model based on the firing technique and employing the Runge-Kutta method.

c) Developing a MATLAB code to provide light on the matter at hand.

d) Analyzing the effect of various physical properties on the profiles of the temperature velocity ,and concentration Casson-Nano-Williamson fluid flow boundary layer.

e) Numerically Heat Transfer and Skin-friction values rate, and mass transfer coefficients are shown in tables as a function of changes in various technical factors.

f) Validation of the numerical approach by research into similar works.

2. Flow Governing Equations

This study examines, magnetic field presence and the melting heat transfer effect, the Brownian motion and thermophoresis effects on a continuous, two-dimensional, electrically conducting,

and incompressible, viscous of Williamson-Casson-nanofluid flow approaching an impermeable extendable sheet. In Fig. 1, the fluid flow's flow shape is shown. The following presumptions are taken into account for this research project:

i. The stretching surface's the x-axis is used to measure it in motions direction , while the minor y-axis is parallel to it.

ii. A velocity ax used to stretch the plate along the x-axis. where a > 0 is stretching parameter.

iii. At the boundary layer occurs at y ≥ 0, here the coordinate is generally supplied for the stretching surface

iv. The melting surface is thought to be at a temperature. Tm and the the temperature of free-stream is T∞,where (T∞>Tm), the fraction of nanoparticle Cw is at the stretching surface assumed constant.

v. The ambient value of nanoparticle fraction is denoted by C∞, When y reaches to infinity

vi. The convective and steady Williamson- The outer layer and the flow of Casson-nanofluid when a uniform magnetic intensity field Bo is present.

vii. Assumed the magnetic Reynoldsnumber is small and This makes the induced magnetic field insignificant.

viii. In the present momentinvestigation, the nanoparticles are moved around in the fluid base in accordance with thermophoresis and Brownian motion.

ix. The temperature and concentration of Thenanoparticle volume and on the boundaries considered to be and , at the wall, and , correspondingly are a long way from the wall..

x. The rheological equation for non-Newtonian fluid is given as, $\tau = \tau_o + \mu\alpha^*$ (1)

xi. Eq. (1)can be expanded asFor Casson fluid,

$$\tau_{ij} = \begin{cases} 2\left(\mu_B + \dfrac{p_y}{\sqrt{2\pi}}\right)e_{ij}, & \pi > \pi_c \\ \& \\ 2\left(\mu_B + \dfrac{p_y}{\sqrt{2\pi_c}}\right)e_{ij}, & \pi < \pi_c \end{cases} \qquad (2)$$

Where $\pi = e_{ij}e_{ji}$ with e_{ij} is the $(i, j)^{th}$ deformation rate of fluid, a component, and $p_y = \dfrac{\mu_B\sqrt{2\pi}}{\beta}$ is the Casson fluid yield stress

Casson-Nano-Williamson fluid

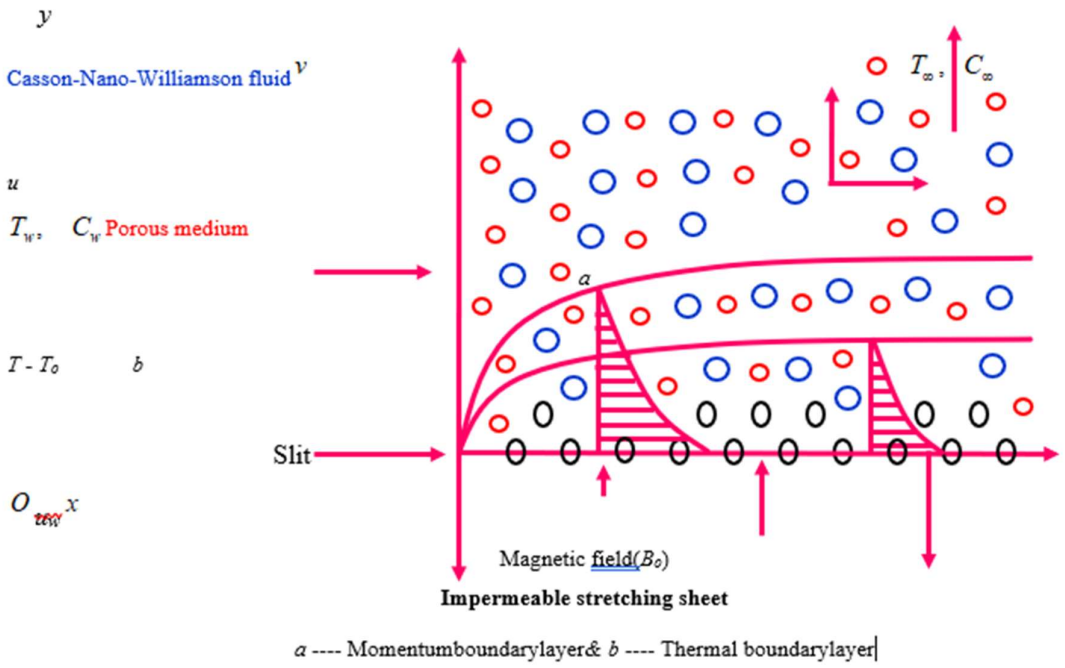

Fig. 1.:The fluid 's Geometry representation

For a steadiness, electrical conductivity, and incompressibility of a casson-nanofluidflow, the boundary layer equations are as follows

Equation of the Continuity:

$$\frac{\partial u}{\partial x}+\frac{\partial v}{\partial y}=0, \tag{3}$$

Equation of the Momentum:

$$u\frac{\partial u}{\partial x}+v\frac{\partial u}{\partial y}=\nu\left(1+\frac{1}{\beta}\right)\frac{\partial^2 u}{\partial y^2}+\sqrt{2}\nu\Gamma\frac{\partial u}{\partial y}\frac{\partial^2 u}{\partial y^2}-\frac{\sigma B_o^2}{\rho}u-\nu\frac{u}{k_1}, \tag{4}$$

Equation of the thermal energy:

$$u\frac{\partial T}{\partial x}+v\frac{\partial T}{\partial y}=\alpha_m\frac{\partial^2 T}{\partial y^2}+\tau_B\left\{D_B\frac{\partial C}{\partial y}\frac{\partial T}{\partial y}+\frac{D_T}{T_\infty}\left(\frac{\partial T}{\partial y}\right)^2\right\}, \tag{5}$$

Equation of the species nanoparticle volume concentration:

$$u\frac{\partial C}{\partial x}+v\frac{\partial C}{\partial y}=D_B\frac{\partial^2 C}{\partial y^2}+\frac{D_T}{T_\infty}\frac{\partial^2 T}{\partial y^2}, \tag{6}$$

For this flow The boundary conditions are

$$\left.\begin{aligned} &u=u_w(x)=ax,\ T=T_m,\ \kappa\left(\frac{\partial T}{\partial y}\right)_{y=0}=\rho\left(\gamma+C_s\left(T_m-T_o\right)\right)v(x,\ 0),\ C=C_w\ \ at\ \ y=0\\ &u\to 0,\ T\to T_\infty,\ C\to C_\infty\ \ as\ \ y\to\infty \end{aligned}\right\} \tag{7}$$

The following similarity transformation can be used to convert the governing equations into ordinary dirivable equations.

$$\left.\psi=\sqrt{a\nu}xf\left(\eta\right),\ \eta=y\sqrt{\frac{a}{\nu}},\ \theta=\frac{T-T_m}{T_\infty-T_m},\ \phi=\frac{C-C_\infty}{C_w-C_\infty}\right\}, \tag{8}$$

The stream function ψ is defined such that $u=\dfrac{\partial\psi}{\partial y}$ and $v=-\dfrac{\partial\psi}{\partial y}$ (9)

equation (3) is identically satisfied, and equations (4), (5) and (6) along with boundary conditions (7) With the help of above transformations take the following forms

$$\left(1+\frac{1}{\beta}\right)f'''+ff''-\left(f'^2\right)+\lambda f''f'''-\left(M+K\right)f'=0, \tag{10}$$

$$\frac{1}{\mathrm{Pr}}\theta''+f\theta'+Nb\theta'\phi'+Nt\theta'^2=0, \tag{11}$$

$$\frac{1}{Nb}\phi''+Lef\phi'+\frac{Nt}{Nb}\theta''=0, \tag{12}$$

the associated boundary conditions (7) become

$$\left.\begin{array}{l}f'\left(0\right)=1,\ Me\theta'\left(0\right)+\mathrm{Pr}\,f\left(0\right)=0,\ \theta\left(0\right)=0,\ \phi\left(0\right)=1\\ f'\left(\infty\right)\to0,\ \theta\left(\infty\right)\to1,\ \phi\left(\infty\right)\to0\end{array}\right\}, \tag{13}$$

where the involved physical parameters are defined as

$$\left.\begin{array}{l}M=\dfrac{\sigma B_o^2}{\rho a},\ K=\dfrac{\nu}{ak_1},\ \lambda=\Gamma x\sqrt{\dfrac{2a^3}{\nu}},\ \mathrm{Pr}=\dfrac{\nu}{\alpha_m},\ Nb=\dfrac{\tau_B D_B\left(C_w-C_\infty\right)}{\nu},\\ Le=\dfrac{\nu}{D_B},\ Nt=\dfrac{\tau_B D_T\left(T_\infty-T_m\right)}{\nu T_\infty},\ Me=\dfrac{C_f\left(T_\infty-T_m\right)}{\gamma+C_s\left(T_m-T_o\right)}\end{array}\right\}, \tag{14}$$

The amounts of interest physically likecoefficient of the Skin-friction (*Cf*) local Nusselt number (*Nu*) and local Sherwood number (*Sh*), as defined

$$C_f=\frac{\tau_w}{\rho u_w^2}=\frac{1}{\rho u_w^2}\left\{\mu\left(\frac{\partial u}{\partial y}\right)_{y=0}+\frac{\Gamma}{\sqrt{2}}\left(\frac{\partial u}{\partial y}\right)_{y=0}^2\right\}\Rightarrow Cf=C_f\left(\sqrt{\mathrm{Re}_x}\right)=f''\left(0\right)+\frac{\lambda}{2}\left\{f''\left(0\right)\right\}^2 \tag{15}$$

$$Nu_x=\frac{xq_w}{\kappa\left(T_\infty-T_m\right)}=-\frac{x\kappa\left(\dfrac{\partial T}{\partial y}\right)_{y=0}}{\kappa\left(T_\infty-T_m\right)}\Rightarrow Nu=Nu_x\left(\mathrm{Re}_x\right)^{\frac{-1}{2}}=-\theta'\left(0\right) \tag{16}$$

$$Sh_x=\frac{xq_m}{D_B\left(C_w-C_\infty\right)}=-\frac{D_B\left(\dfrac{\partial C}{\partial y}\right)_{y=0}}{\left(C_w-C_\infty\right)}\Rightarrow Sh=Sh_x\left(\mathrm{Re}_x\right)^{\frac{-1}{2}}=-\phi'\left(0\right) \tag{17}$$

3. Solution Method byRunge-Kutta method:

A complete set of Eqs .(10)-(12) does not appear to allow for a precise answeras a result of the non-linear character of (10)-(12), providing appropriate conditions boarderlyin (13) and the requirement for numerical approaches to tackle the issue.The controlling derivable equationspartially are changedinto a collection of equations that are ordinary non-linear derivable equationsmay be numericallysolved using a similarity transformation. To solve the ensuing boundary value problem numerically, the shooting approach is combined with a Runge-Kuttafourth-order approach. The nonlinear derivable equations are broken down into a group of dirivable equations of first-order to produce the collection of differential equationsfirst-order. According to the image, the associated ordinary differential equations (10)-(12) into a collection of seven concurrent equations with seven unknowns. Equations of ordinary differential couples (10)-(12) are being cubic order in $f(\eta)$ and second order in $\theta(\eta)$ and $\phi(\eta)$ They have been condensed into a set of multiple equations using seven variousunknowns. There are seven starting conditions needed in order to solve this system of equations numerically with the Runge-Kutta technique. nonetheless, there are two prerequisites in $f(\eta)$ one initial condition in each of $\theta(\eta)$ and $\phi(\eta)$ are known. Although the values of $f'(\eta)$,$\theta(\eta)$ and $\phi(\eta)$ are known at $\eta \to \infty$. These end conditions are utilized to create uncertain starting circumstances at $\eta = 0$ by using shooting technique. The most crucial step in implementing this plan is selecting the suitable finite value of η_∞. Thus to estimate the value of η_∞The boundary value problem, which is composed of Eqs(10)-(12), is first solved using a first guess value. To obtain $f''(0), \theta'(0)$ and $\phi'(0)$. The process of the solution

is repeated with another higher value of η_∞ until two successive values of $f''(0), \theta'(0)$ and $\phi'(0)$ differ only after desired significant digit. The last value η_∞ is using the smallest possible value of the limit η_∞ given the specific set of physical conditions for determining velocity, temperature and, respectively, are $f(\eta)$, $\theta(\eta)$ and $\phi(\eta)$ in the boundary layer. After obtaining all of the starting circumstances, we resolve this system of simultaneous equations using Runge-Kutta fourth order integration scheme. The value of $\eta_\infty$is selected to 8depending on the physical parameters governing the flow so that no numerical oscillation would occur. Consequently, the linked third-order boundary value issue in $f(\eta)$, second-order in $\theta(\eta)$ and $\phi(\eta)$ has been reduced to a system of seven simultaneous first-order equations of for seven unknowns as follows:

$$\left.\begin{aligned} & f' = p \Rightarrow f'' = p' = q \Rightarrow f''' = p'' = q' \Rightarrow q' = \frac{p^2 - \lambda qq' + (M+K)p - fq}{\left(1+\frac{1}{\beta}\right)} \\ & \theta' = r \Rightarrow \theta'' = r' \text{ then } r' = -(\Pr)(Nb)rz - (\Pr)(Nt)r^2 - (\Pr)fr \\ & \& \\ & \phi' = z \Rightarrow \phi'' = z' \text{ then } z' = -(Le)(Nb)fz - (Nt)r' \end{aligned}\right\} (18)$$

and the associated boundary conditions changed

$$p(0) = 1,\ Me\, r(0) + \Pr f(0) = 0,\ \theta(0) = 0,\ \phi(0) = 0,\ p(\infty) \to 0,\ \theta(\infty) \to 1,\ \phi(\infty) \to 1 (19)$$

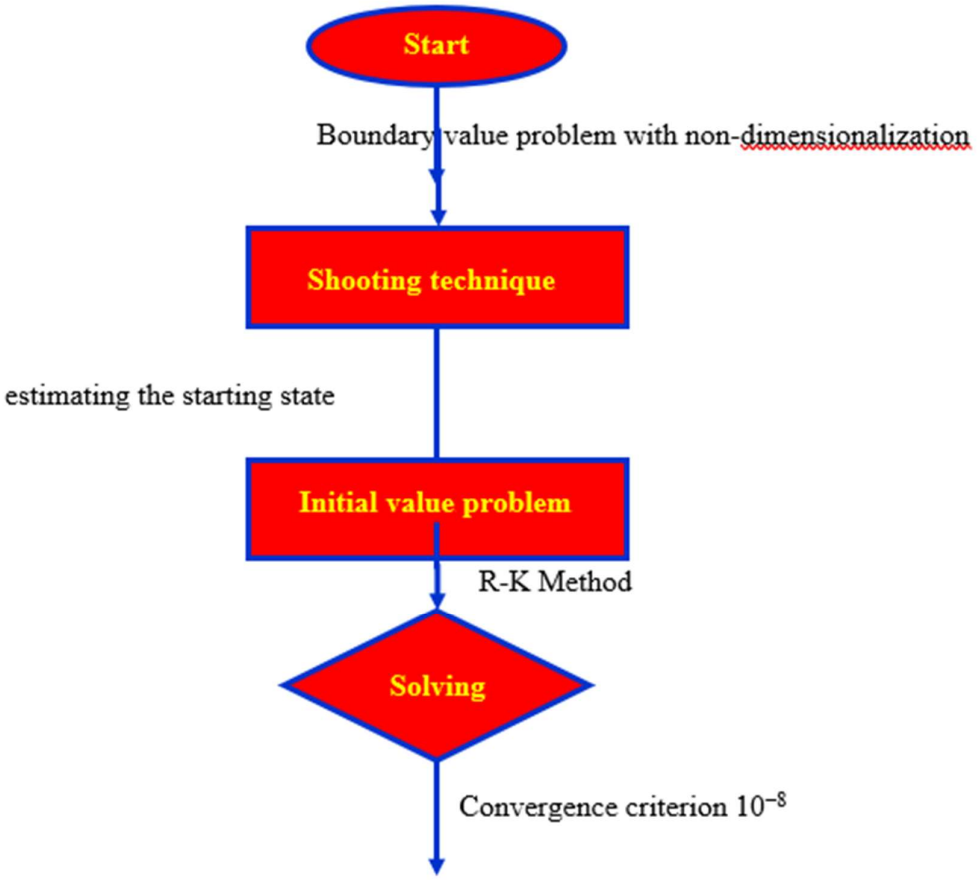

Fig. 2.: Flow diagram of the numerical procedure

Prior to further investigation, first an initial value is created from the boundary value problem. issue. (IVP). The shooting approach is then applied repeatedly until the situation is resolved in order to properly approximate the omitted initial value for different combinations of elements. For purposes of calculation, the step size in this case is h = 0.1. Additionally, a 10-6It is used to tolerate mistake. The material is provided in tables and graphs, with a thorough examination of the difficulties' key characteristics.

4. Program Code Validation:

Table-1.: Comparison of heat transmission rates at present coefficient results with published results of Wang [31], Sidawi and Gorla [32] and Pop and Khan [33] when Nb = Nt = 0

Pr	Wang [31]	Gorla and Sidawi [32]	Khan and Pop [33]	Present results
0.07	0.0656	0.0656	0.0663	0.0659881021
0.20	0.1691	0.1691	0.1691	0.1687550267
0.70	0.4539	0.5349	0.4539	0.4526550399
2.00	0.9114	0.9114	0.9113	0.9112862019

7.00	1.8954	1.8905	1.8954	1.8948527301
20.00	3.3539	3.3539	3.3539	3.3538962175
70.00	6.4622	6.4622	6.4621	6.4620982005

Table-2.: The comparison of recent and published Nusselt number results of Khan and Pop [33] for M = K = Me = λ = 0 and β → ∞

Nt	Khan and Pop [33] results			Present Nusselt number results		
	Nb = 0.1	*Nb* = 0.2	*Nb* = 0.3	*Nb* = 0.1	*Nb* = 0.2	*Nb* = 0.3
0.1	0.9524	0.5056	0.2522	0.9492201355	0.5048862165	0.2520932659
0.2	0.6932	0.3654	0.1816	0.6852201999	0.3648966214	0.1815990554
0.3	0.5201	0.2731	0.1355	0.5189330157	0.2698331567	0.1354699720

Table-3.: The Comparison of current Sherwood outcomes with published findings of Khan and Pop [33] for $M = K = Me = \lambda = 0$ and $\beta \to \infty$

Nt	Khan and Pop [33] results			Present Sherwood number results		
	Nb = 0.1	*Nb* = 0.2	*Nb* = 0.3	*Nb* = 0.1	*Nb* = 0.2	*Nb* = 0.3
0.1	2.1294	2.3819	2.4100	2.1198662015	2.3799502364	2.4089962045
0.2	2.2740	2.5152	2.5150	2.2684403277	2.5189920326	2.5179662034
0.3	2.5286	2.6555	2.6088	2.5199620321	2.6489331771	2.5983001477

In order to verifyprogram code validation ofpresentresults There is a comparison of the most recent outcomes with those that have been released inWang [31], Gorla and Sidawi [32] and Khan and Pop [33]. This comparison is shown in the tables 1, 2 and 3 where a very well agreement been seen in both outcomes and has thus confirmed The reliability of the present findings.

5. Results informationand Discussion Analysis:

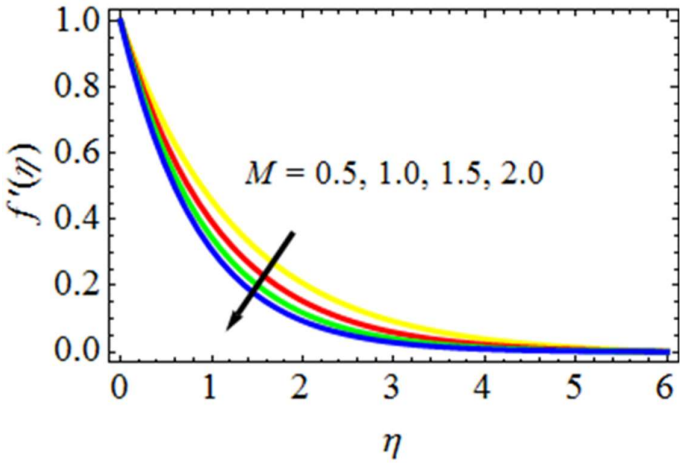

Fig. 3. velocity profiles with the M effect

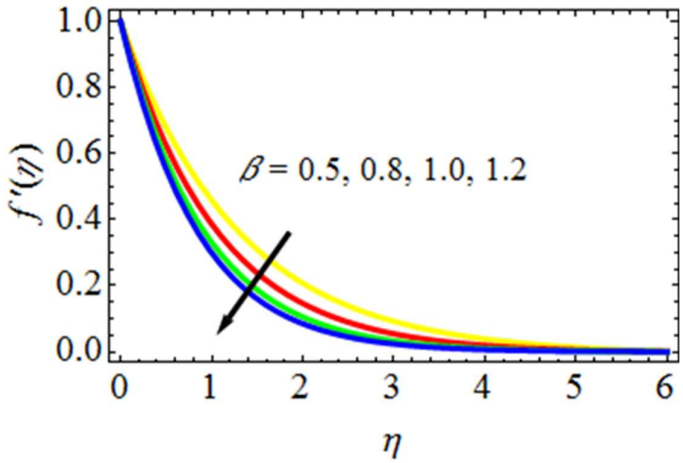

Fig. 4.βeffect on velocity profiles

This study's objectives are to (i) I examine the effects of the relevant factors on the Casson-Williamson flow including nanoparticles; (ii) to find out if there are any numerical solutions; and (iii) to validate the kind of the solution. The discussion and outcomes related to the goal will thus be illuminatedin this paragraph. The numerical results are determined using the following control parameters solutions ofvelocity,temperature,and concentration profiles: M for the magnetic field ($0.5 \leq M \leq 2.0$) , Casson parameter β ($0.5 \leq \beta \leq 1.2$), Permeability parameter K ($0.5 \leq K \leq 1.5$), Williamson parameter λ ($0.5 \leq \lambda \leq 2.0$), Prandtl Number Pr ($0.71 \leq Pr \leq 7.0$), Melting parameter Me ($0.3 \leq Me \leq 1.0$), Parameter for Brownian motion Nb ($0.3 \leq Nb \leq 1.0$), parameter of thermophoresis Nt($0.5 \leq Nt \leq 1.5$), Lewis number Le ($0.5 \leq Le \leq 1.2$) are investigated and illustrated in Figs. 3, 4, 5, 6, 7, 8, 9, 10, 11, 12, 13 and Tables 3, 4, 5 and 6 respectively.

- Fig. 3display the impact of the M magnetic field parameter ($0.5 \leq M \leq 2.0$) on velocity profiles.Our ability to reduce that the fluid's velocity decreased as the 0.5, 1.0, 1.5, and 2.0. This is because the magnetic field produces a decelerating body it is aa Lorentz force, In

contrast to the magnetic field's direction of action. This bodily power causes a decrease in the thickness and flow momentum boundary layer. Similar to that, it produces heatdue tothe Lorentz force, a minimal resistive force opposing the fluid's velocity. This characteristic causes when the magnetic field is stronger thenthe thermal boundary layer to be thicker.

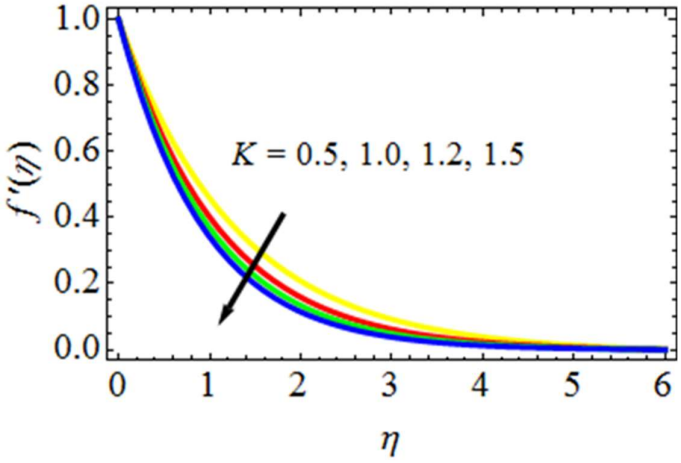

Fig. 5.Impact of K on velocity profiles

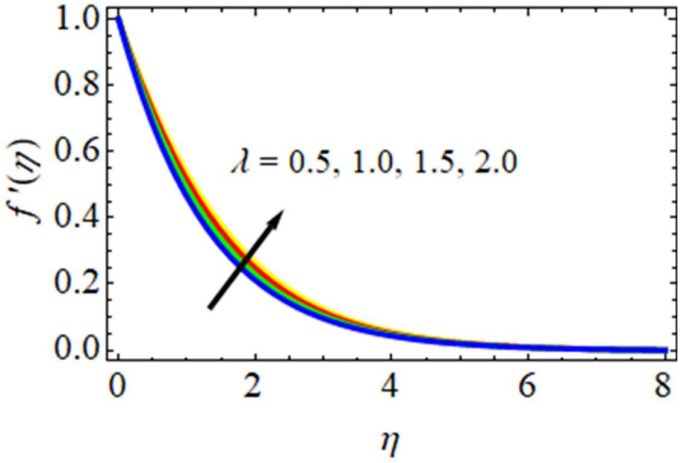

Fig. 6.Impact of λ on velocity profiles

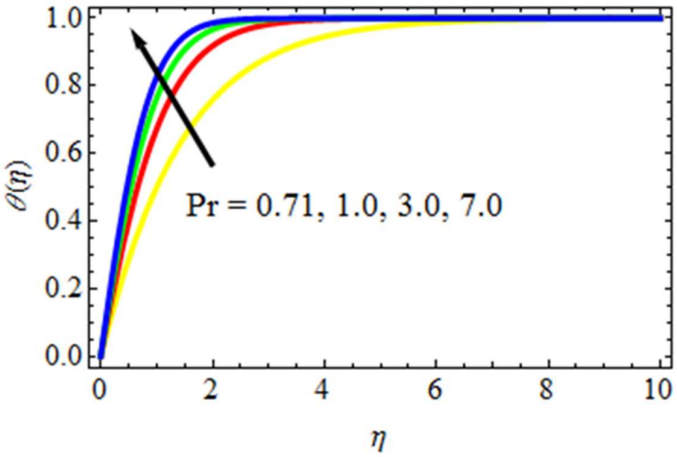

Fig. 7.Preffect on temperature profiles

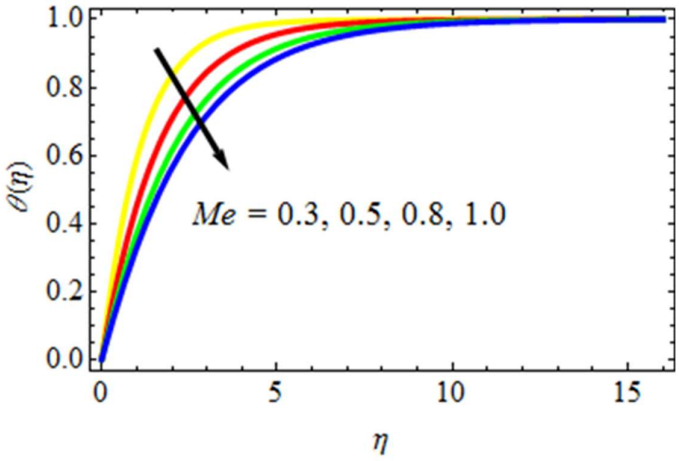

Fig. 8.Impact of Me on temperature profiles

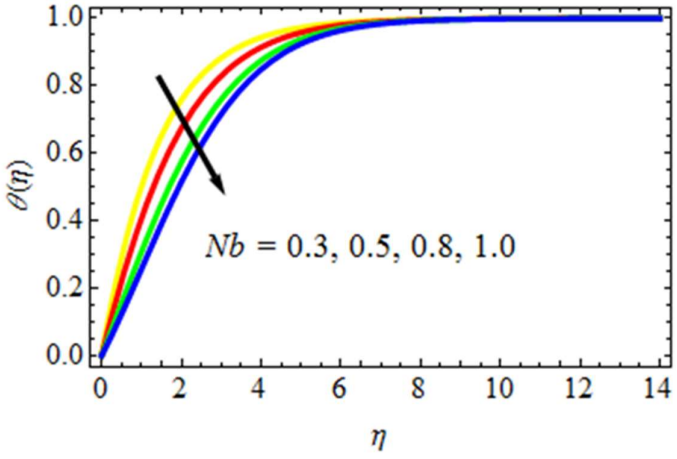

Fig. 9. Impact of Nb on temperature profiles

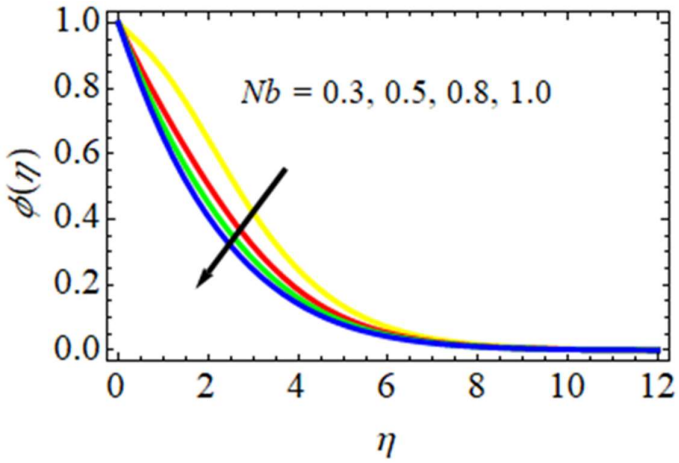

Fig. 10.Impact of Nb on concentration profiles

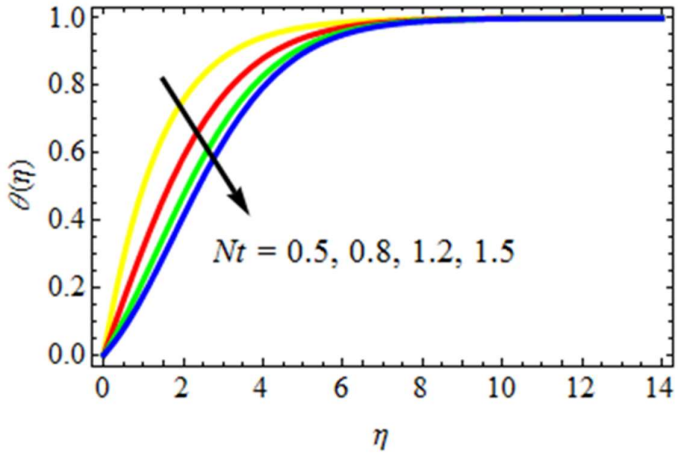

Fig. 11.Impact of Nton temperature profiles

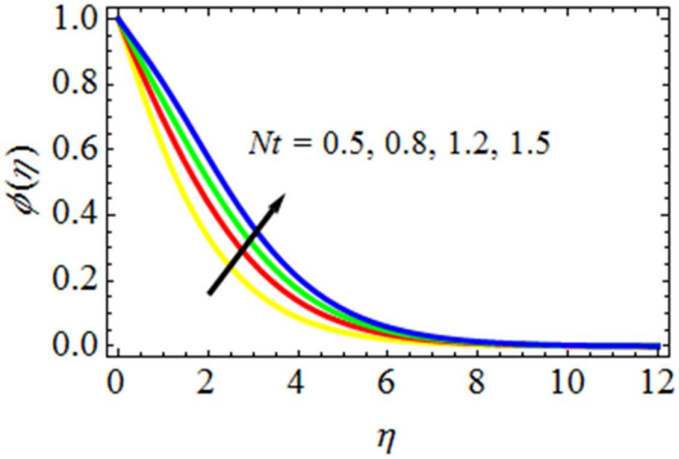

Fig. 12.Impact of Nton concentration profiles

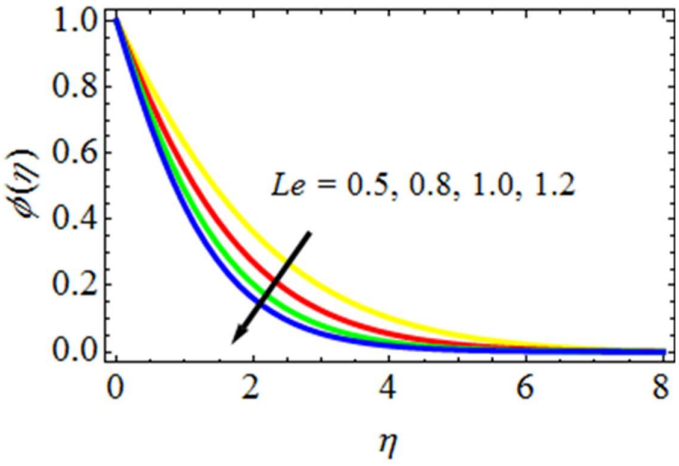

Fig. 13.Impact of Le on concentration profiles

- The impact of Casson parameter β(0.5 ≤β ≤ 1.2) on profiles of velocity is shown in Fig. 4. It is looked at if stream-wise velocity profiles decrease as the Casson parameter increases. It may be explained by saying that surfaces close to the sheet's velocity display rising behaviour because slip boundary conditions exist. Thestress of the yield decreases as the result of a rise in the Casson parameter, which makes it easier for fluid components to move through the fluid.
- Fig. 5 demonstrates the effect of Permeability parameter K (0.5 ≤K ≤1.5) about velocity profiles. It goes without saying that the of porous mediapresence the flow restrictionincreases, which slows the fluid's velocity. As a result, the velocity drops as the parameter permeability increases, increasing the resistance to the fluid motion.
- Fig. 6 presentsthe many non-Newtonian Williamson parameter values λ(0.5 ≤λ ≤2.0) on velocity profiles. The velocity profiles value decreases when Increase in the Williamson parameter Due to suspended nanoparticles' ability to stay longer in the base fluids and improve the flow properties of nanofluids, it is beneficial to use as a lubricant in cooling systems..
- Fig. 7 illustrates impact of Prandtl Number Pr (0.71 ≤ Pr ≤ 7.0). profile of the Temperature is decreased whenincreased the Prandtl number. Thermal diffusivity and the Prandtl parameter consists the relationshipinversely. Less thermal diffusivity is shown by higher Prandtl parameter estimates, which results in a decrease in temperature distribution. The thermal sketch gets smaller as the Prandtl number rises because it tends to reduce thermal diffusivity, which slows down temperature diffusion.
- Fig. 8 reveals distributions of temperature for various Melting parameterMe values(0.3 ≤Me ≤1.0). The temperature and thicknes of the boundary layerare shown to decrease with increaselevels of ‘Me’. This is due to the fact that a rise in Me will increase melting's intensity, which acts as a the boundary layer tends to become thicker due to the blown boundary condition at the stretched surface.
- The impact of the Brownian motion parameter Nb (0.3 ≤Nb ≤1.0) Figs. 9 and 10 respectively display information onthe temperature and concentrationprofiles. The

profile of temperature was brought on by an the Brownian motion parameter is increased to settle at greater values. When base fluid collide and nanoparticles , Brownian motion results, which is random motion. Greater collisions and more parameter of Brownian motion. The internal kinetic energy a rise in the fluid's result of particle contact. The profile of concentration profile and the parameterof Brownian motion are inversely correlated. Theparameter o Brownian motion parameter is greater and fewer nanoparticles are present in the fluidbase..

- Figs. 11 and 12reveal theeffect of thermophoresis parameter Nt($0.5 \leq Nt \leq 1.5$)regarding the profiles of temperature and concentration. Greater levels of Nt result in higher temperature and concentration profiles. Thermophoresis is the transport force brought on by the temperature difference between fluid layers. More Thermophoresis parameters enhance the temperature differential between the layers, increasing the rate of heat conversion in the process. The fluid's concentration rises as the amount of nanoparticles increases. Because heat is transformed between layers more when there are more nanoparticles, Nt causes a rise in both concentration profiles and temperature profiles.
- The number of Lewis Le($0.5 \leq Le \leq 1.2$) is significant in mass transport phenomena. The Lewis number Le is connected to concentration nanoparticles diffusion.. Fig. 13 describes how growing Lewis number Le is used to evaluate the concentration profile. Brownian diffusivity and Lewis parameter are directly inversely proportional. Higher Brownian diffusivity due to a higher Lewis parameter results in a rise in the nanoparticle concentration field.
- Table-4showsthe quantitative Skin-friction coefficient for changes in engineering factors like the Magnetic field parameter M (= 0.5, 1.0, 1.5) , Casson parameter β (= 0.5, 0.8, 1.0), Permeability parameter K (= 0.5, 1.0, 1.2), Williamson parameter λ (= 0.5, 1.0, 1.5), Prandtl Number Pr (= 0.71, 1.0, 3.0), Melting parameter Me (= 0.3, 0.5, 0.8), parameter of Brownian motion Nb (= 0.3, 0.5, 0.8), Thermophoresis parameter Nt(= 0.5, 0.8, 1.2), Lewis number Le(= 0.5, 0.8, 1.0). This table reveals that when the Williamson parameter's values rise, the coefficient of skin-friction rises as well. λ(= 0.5, 1.0, 1.5), Melting parameter Me (= 0.3, 0.5, 0.8), Parameter of Brownian motion Nb (= 0.3, 0.5, 0.8), Thermophoresis ParameterNt(= 0.5, 0.8, 1.2), while it is decreasing with increasing Magnetic field parameter values M(= 0.5, 1.0, 1.5), Casson parameter β (= 0.5, 0.8, 1.0), Permeability parameter K (= 0.5, 1.0, 1.2), Prandtl Number Pr (= 0.71, 1.0, 3.0), Lewis number Le(= 0.5, 0.8, 1.0).
- Using the Nusselt number as a unit of measurement, the numerical rates of coefficient of the heat transfer are shown in Table-6The Prandtl Number for different values Pr (= 0.71, 1.0, 3.0), Melting parameter Me (= 0.3, 0.5, 0.8),Parameter of Brownian motionparameterNb (= 0.3, 0.5, 0.8), Thermophoresis parameter Nt(= 0.5, 0.8, 1.2). With increasing values of the melting parameterMe(= 0.3, 0.5, 0.8), the of heat transfer coefficientrate gradually increases, parameter of Brownian motion Nb (= 0.3, 0.5, 0.8),

Thermophoresis parameter Nt(= 0.5, 0.8, 1.2), is observed that while the opposite result raises Prandtl Number values Pr (= 0.71, 1.0, 3.0).

- The impact ofparameterof Brownian motionNb (= 0.3, 0.5, 0.8), Thermophoresis parameter Nt(= 0.5, 0.8, 1.2), Lewis number Le(= 0.5, 0.8, 1.0)In Table 7, it is described how themass transfer coefficient rate or the coefficient Sherwood number rate. This table shows that the coefficient rate of mass transfer rises as the value of the thermophoresis parameterNt(= 0.5, 0.8, 1.2) increases.and declining as theincreased values of parameter Brownian motionNb(= 0.3, 0.5, 0.8), Lewis number Le(= 0.5, 0.8, 1.0).

Table-4.: Values of Skin-friction coefficient in Numerical

M	*β*	*K*	*Λ*	*Le*	Pr	*Me*	*Nb*	*Nt*	*Cf*
0.5	0.5	0.5	0.5	0.5	0.71	0.3	0.3	0.5	1.5581220154
1.0									1.4988302678
1.5									1.4599017874
	0.8								1.5236698219
	1.0								1.5098831775
		1.0							1.5199728453
		1.2							1.4964002371
			1.0						1.5862249756
			1.5						1.6087510493
				0.8					1.5187556044
				1.0					1.4985037412
					1.00				1.4893327741
					7.00				1.4699307751
						0.5			1.5786622495
						0.8			1.5973360457
							0.5		1.5799630196
							0.8		1.5986642281
								0.8	1.5894463209
								1.2	1.6099832145

Table-5.: Numerical values for therate of heat transfer coefficient

Pr	*Me*	*Nb*	*Nt*	*Nu*
0.71	0.3	0.3	0.5	0.7886215954
1.00				0.7059962179
7.00				0.6873306441
	0.5			0.8156621893

	0.8			0.8399741562
		0.5		0.8099422134
		0.8		0.8277634889
			0.8	0.8178795546
			1.2	0.8366520078

Table-6.: Values of rate of mass transfer coefficient in Numerical

Le	*Nb*	*Nt*	*Sh*
0.5	0.3	0.5	0.7488203658
0.8			0.7054410698
1.0			0.6872214593
	0.5		0.7156634471
	0.8		0.6863204124
		0.8	0.7699312455
		1.2	0.7820136549

6. Conclusions:

In the existing research manuscript, the effects of both of Melting heat transfer and Porous medium on a 2-D steady boundary layer Casson-Williamsonflow-flow of Nano fluid over a linearly extending a sheet in the presence a field of magnetic, effects of theThermophoresis, Brownian motion quantitatively examined.Themethod of Runge-Kutta and shooting technique are used to resolve the rewritten, nonlinear ordinary solvable equations numerically controlling the flow. For different values of the main engineering parameters, the graphical results of the numerically computed results for, temperature,velocity, and concentration distributions are shown. Also looked at is how different factors affect the Skin-friction, numbers likeNusselt andSherwood.

The following is summary of most significant findings:

- The profiles of velocity are decreaseswith increased magnetic parameter levels because Lorentz force.
- The profiles of velocity are reduced in order to raise the Cason fluid parameter and Permeability parameter values.
- With an improvement in melting heat transfer parameter and theparameter of the thermophoresis, the thickness of boundary layer of the temperature profiles rise..
- With Temperature profile increases for increasing values of Brownian motion parameter
- Brownian motion parametervaluesincreases and Lewis number and the concentration profiles,are decreases whereas the profiles of concentration are increasing with increase of Thermophoresis parameter.
- DecreasesTemperature profile for of Prandtl numberincreasing values.

- The current outcomes are excellent and represent Wang[31] in a more complete manner., Gorla and Sidawi [32] and Khan and Pop [33].
- In future, the authors have toplan To build on this work by examining mass and heat fluxes in order to regulate the cooling process with a non-Newtonian nanofluid.

References:

1. S. U. S. Choi, Enhancing thermal conductivity of fluids with nanoparticles, D. A. Siginer, H. P. Wang (Eds.), Developments and Applications of Non-Newtonian Flows, ASME, New York (1995), pp. 99-105.
2. T. Hayat, A. Aziz, T. Muhammad, B. Ahmad, Influence of magnetic field in three-dimensional flow of couple stress nanofluid over a nonlinearly stretching surface with convective condition, PLOS ONE, 10 (12) (2015), p. e0145332.
3. H. Zargartalebi, M. Ghalambaz, A. Noghrehabadi, A.J. Chamkha, Stagnation-point heat transfer of nanofluids toward stretching sheets with variable thermo-physical properties, Adv. Powder Technol., 26 (3) (2015), pp. 819-829, 10.1016/j.apt.2015.02.008.
4. S. Nadeem, M.R. Khan, A.U. Khan, MHD stagnation point flow of viscous nanofluid over a curved surface, Phys. Scripta, 94 (11) (2019), Article 115207.
5. Ch. Ram Reddy, P.V.S.N. Murthy, A.J. Chamkha, A.M. Rashad, Soret effect on mixed convection flow in a nanofluid under convective boundary condition, Int. J. Heat Mass Transf., 64 (2013), pp. 384-392.
6. A. Zaraki, M. Ghalambaz, A.J. Chamkha, M. Ghalambaz, D. De Rossi, Theoretical analysis of natural convection boundary layer heat and mass transfer of nanofluids: effects of size, shape and type of nanoparticles, type of base fluid and working temperature, Adv. Powder Technol. 26 (2015) 935–946.
7. R.K. Tiwari, M.K. Das, Heat transfer augmentation in a two-sided lid-driven differentially heated square cavity utilizing nanofluids, Int. J. Heat Mass Transf., 50 (2007), pp. 2002-2018.
8. R.S.R. Gorla, A.J. Chamkha, V. Ghodeswar, Natural convective boundary layer flow over a vertical cone embedded in a porous medium saturated with a nanofluid, J. Nanofluids, 3 (2014), pp. 65-71.
9. S. Nadeem, R. Mehmood, N.S. Akbar, Partial slip effect on non-aligned stagnation point nanofluid over a stretching convective surface, Chin. Phys. B, 24 (1) (2015), pp. 1-8.
10. M.A. Sheremet, I. Pop, Conjugate natural convection in a square porous cavity filled by a nanofluid using Buongiorno′s mathematical model, Int. J. Heat Mass Transf., 79 (2014), pp. 137-145.
11. R.U. Haq, Z.H. Khan, W.A. Khan, Thermophysical effects of carbon nanotubes on MHD flow over a stretching surface, Phys. E Low-dimens. Syst. Nanostruct., 63 (2014), pp. 215-222.

12. P. Sudarsana Reddy, A.J. Chamkha, Heat and mass transfer analysis in natural convection flow of nanofluid over a vertical cone with chemical reaction, Int. J. Numer. Methods Heat Fluid Flow, 27 (1) (2017), pp. 1-22.
13. O.D. Makinde, A. Aziz, Boundary layer flow of a nanofluid past a stretching sheet with a convective boundary condition, Int. J. Therm. Sci., 50 (2011), pp. 1326-1332.
14. A. J. Chamkha, A.M. Rashad, Ch. Ram Reddy, P.V. Murthy, Effect of suction/injection on free convection along a vertical plate in a nanofluid saturated non-Darcy porous medium with internal heat generation, Indian J. Pure Appl. Math., 45 (2014), pp. 321-341.
15. E. Abu-Nada, H.F. Oztop, Effects of inclination angle on natural convection in enclosures filled with Cu-water nanofluid, Int. J. Heat Fluid Flow, 30 (2009), pp. 669-678.
16. R. Vo. Williamson, The flow of pseudoplastic materials,Ind. Eng. Chem., 21 (11) (1929), pp. 1108-1111.
17. M. Bhatti, M. Arain, A. Zeeshan, R. Ellahi, M. Doranehgard, Swimming of gyrotactic microorganism in MHD Williamson nanofluid flow between rotating circular plates embedded in porous medium: Application of thermal energy storage, Journal of Energy Storage (2021), p. 103511.
18. Loganathan K., Rajan S., An entropy approach of Williamson nanofluid flow with joule heating and zero nanoparticle mass flux, J. Therm. Anal. Calorim., 141 (6) (2020), pp. 2599-2612.
19. Sreedevi P., Reddy P. S., Williamson hybrid nanofluid flow over swirling cylinder with Cattaneo-Christov heat flux and gyrotactic microorganism, Waves Random Complex Media (2021), pp. 1-28.
20. M. Amer Q., Numerical simulation of heat transfer flow subject to MHD of Williamson nanofluid with thermal radiation, Symmetry, 13 (1) (2020), p. 10.
21. Yahya A.U., Salamat N., Habib D., Ali B., Hussain S., Abdal S., Implication of bio-convection and Cattaneo-Christov heat flux on Williamson sutter by nanofluid transportation caused by a stretching surface with convective boundary, Chinese J. Phys., 73 (2021), pp. 706-718.
22. K. Ahmed, W. A. Khan, T. Akbar, G. Rasool, S. O. Alharbi, I. Khan, Numerical investigation of mixed convective Williamson fluid flow over an exponentially stretching permeable curved surface, Fluids, 6 (7) (2021), p. 260.
23. A. Aldabesh, S. U. Khan, D. Habib, H. Waqas, I. Tlili, M. I. Khan, W. A. Khan, Unsteady transient slip flow of Williamson nanofluid containing gyrotactic microorganism and activation energy, Alexandr. Eng. J., 59 (6) (2020), pp. 4315-4328.
24. Krishnamurthy M. R., Prasannakumara B. C., Gireesha B. J., Gorla R. S. R., Effect of chemical reaction on MHD boundary layer flow and melting heat transfer of Williamson nanofluid in porous medium, Eng. Sci. Technol., 19 (1) (2016), pp. 53-61.
25. G. Kumaran, N. Sandeep, and R. Vijayaragavan, Melting heat transfer in magnetohydrodynamic radiative Williamson fluid flow with non-uniform heat

source/sink,IOP Conference Series: Materials Science and Engineering, vol. 263, no. 6. IOP Publishing, 2017, p. 062022.

26. Dawar A., Shah Z., Islam S., Khan W., Idrees M., An optimal analysis for Darcy-Forchheimer three-dimensional Williamson nanofluid flow over a stretching surface with convective conditions, Adv. Mech. Eng., 11 (3) (2019), Article 1687814019833510.
27. M. Azam, F. Mabood, T. Xu, M. Waly, I. Tlili, Entropy optimized radiative heat transportation in axi-symmetric flow of Williamson nanofluid with activation energy, Results in Physics, 19 (2020), p. 103576.
28. C. S. Raju, N. Sandeep, M. E. Ali, A. O. Nuhait, Heat and mass transfer in 3-d MHD Williamson-casson fluids flow over a stretching surface with non-uniform heat source/sink, Thermal Science, 23 (1) (2019), pp. 281-293.
29. Shafiq A., Sindhu T. N., Statistical study of hydromagnetic boundary layer flow of Williamson fluid regarding a radiative surface, Results Phys., 7 (2017), pp. 3059-3067.
30. U. Nazir, M. A. Sadiq, M. Nawaz, Non-Fourier thermal and mass transport in hybridnano-Williamson fluid under chemical reaction in Forchheimer porous medium, Int. Commun. Heat Mass Transfer, 127 (2021), p. 105536.
31. C.Y. Wang, Free convection on a vertical stretching surface, J. Appl. Math.Mech. (ZAMM) 69 (1989) 418–420.
32. R.S.R. Gorla, I. Sidawi, Free convection on a vertical stretching surface withsuction and blowing, Appl. Sci. Res. 52 (1994) 247–257.
33. W.A. Khan, I. Pop, Boundary-layer flow of a nanofluid past a stretching sheet,Int. J. Heat Mass Transf. 53 (2010) 2477–2483.